Warm FIRE: simulating galaxy formation with resonant sterile neutrino dark matter

Bozek, Brandon ; Fitts, Alex ; Boylan-Kolchin, Michael ; Garrison-Kimmel, Shea ; Abazajian, Kevork ; Bullock, James S ; Kereš, Dušan ; Faucher-Giguère, Claude-André ; Wetzel, Andrew ; Feldmann, Robert ; Hopkins, Philip F

Abstract: We study the impact of a warm dark matter (WDM) cosmology on dwarf galaxy formation through a suite of cosmological hydrodynamical zoom-in simulations of Mhalo 1010M dark matter haloes as part of the Feedback in Realistic Environments (FIRE) project. A main focus of this paper is to evaluate the combined effects of dark matter physics and stellar feedback on the well-known small-scale issues found in cold dark matter (CDM) models. We find that the z = 0 stellar mass of a galaxy is strongly correlated with the central density of its host dark matter halo at the time of formation, zf, in both CDM and WDM models. WDM haloes follow the same M (z = 0)–Vmax(zf) relation as in CDM, but they form later, are less centrally dense, and therefore contain galaxies that are less massive than their CDM counterparts. As a result, the impact of baryonic effects on the central gravitational potential is typically diminished relative to CDM. However, the combination of delayed formation in WDM and energy input from stellar feedback results in dark matter profiles with lower overall densities. The WDM galaxies studied here have a wider diversity of star formation histories (SFHs) than the same systems simulated in CDM, and the two lowest M WDM galaxies form all of their stars at late times. The discovery of young ultrafaint dwarf galaxies with no ancient star formation – which do not exist in our CDM simulations – would therefore provide evidence in support of WDM.

DOI: https://doi.org/10.1093/mnras/sty3300

Monthly Notices
of the
ROYAL ASTRONOMICAL SOCIETY

MNRAS **483,** 4086–4099 (2019)
Advance Access publication 2018 December 12

doi:10.1093/mnras/sty3300

Warm FIRE: simulating galaxy formation with resonant sterile neutrino dark matter

Brandon Bozek,[1]★ Alex Fitts,[1] Michael Boylan-Kolchin [1]★
Shea Garrison-Kimmel [2] Kevork Abazajian [3] James S. Bullock,[3] Dušan Kereš,[4]
Claude-André Faucher-Giguère,[5] Andrew Wetzel [6] Robert Feldmann [7] and
Philip F. Hopkins [2]

[1]*Department of Astronomy, The University of Texas at Austin, 2515 Speedway, Stop C1400, Austin, TX 78712, USA*
[2]*TAPIR, California Institute of Technology, Pasadena, CA 91125, USA*
[3]*Department of Physics and Astronomy, University of California, Irvine, CA 92697, USA*
[4]*Department of Physics, Center for Astrophysics and Space Sciences, University of California, San Diego, La Jolla, CA 92093, USA*
[5]*Department of Physics and Astronomy and CIERA, Northwestern University, 2145 Sheridan Road, Evanston, IL 60647, USA*
[6]*Department of Physics, University of California, Davis, CA 95616, USA*
[7]*Institute for Computational Science, University of Zurich, Zurich CH-8057, Switzerland*

Accepted 2018 November 27. Received 2018 November 16; in original form 2018 March 13

ABSTRACT

We study the impact of a warm dark matter (WDM) cosmology on dwarf galaxy formation through a suite of cosmological hydrodynamical zoom-in simulations of $M_{\rm halo} \approx 10^{10}\,{\rm M}_\odot$ dark matter haloes as part of the Feedback in Realistic Environments (FIRE) project. A main focus of this paper is to evaluate the combined effects of dark matter physics and stellar feedback on the well-known small-scale issues found in cold dark matter (CDM) models. We find that the $z = 0$ stellar mass of a galaxy is strongly correlated with the central density of its host dark matter halo at the time of formation, $z_{\rm f}$, in both CDM and WDM models. WDM haloes follow the same $M_\star(z = 0)$–$V_{\rm max}(z_{\rm f})$ relation as in CDM, but they form later, are less centrally dense, and therefore contain galaxies that are less massive than their CDM counterparts. As a result, the impact of baryonic effects on the central gravitational potential is typically diminished relative to CDM. However, the combination of delayed formation in WDM and energy input from stellar feedback results in dark matter profiles with lower overall densities. The WDM galaxies studied here have a wider diversity of star formation histories (SFHs) than the same systems simulated in CDM, and the two lowest $M_\star$ WDM galaxies form all of their stars at late times. The discovery of young ultrafaint dwarf galaxies with no ancient star formation – which do not exist in our CDM simulations – would therefore provide evidence in support of WDM.

Key words: galaxies: dwarf – galaxies: evolution – galaxies: formation – galaxies: star formation – cosmology: theory – dark matter.

1 INTRODUCTION

The leading class of dark matter particle candidates is phenomenologically 'cold', which is consistent with the weakly interacting massive particle (WIMP) paradigm, axion dark matter, and many other particle physics models. Numerous studies using high-resolution numerical simulations have demonstrated the dark energy + cold dark matter [CDM; (ΛCDM)] model's ability to reproduce the observed properties of the Universe on scales above $\sim$1 Mpc (for recent reviews see Frenk & White 2012; Kuhlen, Vogelsberger & Angulo 2012; Primack 2015). On smaller scales, comparing predictions of the ΛCDM model from dark matter-only (DMO) simulations with observations of low-mass galaxies reveals several issues (Bullock & Boylan-Kolchin 2017). Those issues include the overprediction of low-mass subhaloes compared with counts of dwarf galaxies in the Local Group (Missing Satellites Problem – Klypin et al. 1999; Moore et al. 1999) and a mismatch of the predicted dark matter content of dark matter haloes and the dark matter

★ E-mail: bozek@astro.as.utexas.edu (BB); mbk@astro.as.utexas.edu (MB-K)

density inferred from observations of dwarf galaxies expected to reside in those haloes (the cusp-core Problem – Flores & Primack 1994; Moore 1994 and the Too Big To Fail (TBTF) Problem – Boylan-Kolchin, Bullock & Kaplinghat 2011, 2012). The proposed resolutions of these issues within the context of general relativity appeal to galaxy formation physics altering the predicted dark matter halo properties, new dark matter physics, or some combination of the two effects (for a discussion of these and other issues in the context of modified gravity theories, see Famaey & McGaugh 2012).

Hydrodynamic simulations over a range of scales, from low-mass dwarf galaxies to larger Milky Way-sized galaxies, have demonstrated the importance of baryonic processes in addressing small-scale dark matter issues and building realistic Local Group galaxy populations within the ΛCDM paradigm (Governato et al. 2012; Zolotov et al. 2012; Sawala et al. 2016; Wetzel et al. 2016). For example, the Missing Satellites problem can be remedied by suppressing star formation in low-mass haloes through a combination of stellar feedback and photoionization from a UV background (Bullock, Kravtsov & Weinberg 2000; Benson et al. 2002; Somerville 2002; Kravtsov, Gnedin & Klypin 2004). The discrepancy in counts of luminous satellites and subhaloes can be further alleviated by tidal disruption of dark matter subhaloes in simulations that include a Galactic disc potential (D'Onghia et al. 2010; Garrison-Kimmel et al. 2017b; Sawala et al. 2017; though see van den Bosch et al. 2018). High-resolution hydrodynamical simulations of the Milky Way-mass haloes including these two components have reproduced a satellite stellar mass function that is consistent with observations down to $M_\star \gtrsim 10^5\,\mathrm{M}_\odot$ (Sawala et al. 2016; Wetzel et al. 2016).

The TBTF and cusp-core problems may be resolved via repeated stellar bursts driving baryonic material from halo centres and triggering gravitational potential fluctuations that reduce central dark matter density (Governato et al. 2012; Zolotov et al. 2012; Di Cintio et al. 2014a,b; Chan et al. 2015; Oñorbe et al. 2015; Read, Agertz & Collins 2016; Brooks et al. 2017). However, the input physics and star formation prescriptions of different simulations have resulted in different predictions for the degree to which dark matter structure is modified by stellar feedback events. For example, while Sawala et al. (2016) and Wetzel et al. (2016) both reproduce many observed properties of Local Group galaxies including resolving the TBTF problem, they disagree on whether the inner density profile of dwarf galaxies feature a core or a cusp. Understanding dwarf galaxy formation and evolution is critical to testing both the nature of dark matter and the coupling between dark matter and galaxy formation physics.

Small-scale issues have motivated consideration of warm dark matter (WDM) as a compelling alternative to the standard CDM scenario. WDM models feature the same large-scale predictions of the CDM model, but incorporate a non-negligible velocity distribution that erases primordial perturbations with masses below a model-dependent scale (Hogan & Dalcanton 2000; Barkana, Haiman & Ostriker 2001; Bode, Ostriker & Turok 2001; Sommer-Larsen & Dolgov 2001). Dissipationless WDM simulations have shown that fewer low-mass haloes form as a result thereby addressing the Missing Satellites problem independent of the details of galaxy formation models (Colín, Avila-Reese & Valenzuela 2000; Bode et al. 2001; Polisensky & Ricotti 2011; Lovell et al. 2012; Anderhalden et al. 2013; Bozek et al. 2016; Horiuchi et al. 2016). WDM haloes do not suffer from the TBTF problem to the same degree as they form later with a reduced central density than CDM haloes of similar masses (Lovell et al. 2012; Horiuchi et al. 2016; Lovell et al. 2017a). WDM haloes can also feature cored dark matter density profiles (Tremaine & Gunn 1979; Dalcanton & Hogan 2001), but the free-streaming scales of the models we consider here are not expected to resolve the cusp-core problem (Villaescusa-Navarro & Dalal 2011; Macciò et al. 2012; Shao et al. 2013). For example, a thermal WDM particle with mass, $m_{\rm thm} = 2\,\mathrm{keV}$ is predicted to produce a $r \approx 10\,\mathrm{pc}$ core in a $10^{10}\,\mathrm{M}_\odot$ halo, which falls significantly below the ∼100–1000 pc core size observationally inferred for dwarf galaxies (Gilmore et al. 2007; Oh et al. 2011; Walker & Peñarrubia 2011)

In this work, we consider a specific WDM particle model: a resonantly-produced sterile neutrino (RPSN; Shi & Fuller 1999). In addition to resolving small-scale issues, the RPSN model is motivated as a potential source of the significant, but tentative, detection of a 3.55 keV line in the X-ray flux observed in the centre of the MW, M31, the Perseus cluster, and stacked observations of other clusters (Boyarsky et al. 2014; Bulbul et al. 2014; Boyarsky et al. 2015; Iakubovskyi 2016; Abazajian 2017). A RPSN with the proper mixing angles and a mass of 7.1 keV can radiatively decay into an active neutrino and a $E = 3.55\,\mathrm{keV}$ photon (Shi & Fuller 1999; Abazajian 2014). While both the existence of the line and its interpretation remain controversial, the possibility that the line represents a detection of dark matter makes it a compelling and intriguing signal. As detailed in Section 2, the parametrization of the RPSN model we adopt is consistent with tentative detections of this line in galaxy and galaxy cluster observations while also providing the largest free-streaming effects allowable by observations of small-scale structure (Bose et al. 2016b; Bozek et al. 2016; Horiuchi et al. 2016).

A key threshold for galaxy formation within the CDM paradigm is a halo mass of $10^{10}\,\mathrm{M}_\odot$. This scale corresponds to the transition between mass regimes where stellar feedback is effective (at higher masses) to ineffective (at lower masses) in modifying haloes' central dark matter distributions (Governato et al. 2012; Di Cintio et al. 2014a; Oñorbe et al. 2015). Haloes at this mass are expected to be susceptible to reionization-induced feedback that reduces their baryonic content and subsequently affects the star formation histories (SFHs) of the central galaxies (Efstathiou 1992; Hoeft et al. 2006; Okamoto, Gao & Theuns 2008; Noh & McQuinn 2014). Fitts et al. (2017) studied a suite of haloes at this mass scale and demonstrated the combination of stellar feedback and UV-suppression effects provides a diversity of SFHs that range from continuous star formation to early self-quenching to haloes that do not form any stars by $z = 0$. Consistent with other studies (Di Cintio et al. 2014a; Chan et al. 2015; Tollet et al. 2016), they also identified a critical threshold in the stellar mass-halo mass ratio of 2×10^{-4} for $10^{10}\,\mathrm{M}_\odot$ haloes: haloes above this threshold are able to significantly modify their density profile, while haloes below are not. The resulting galaxies are classical dwarf galaxy analogues with clear predictions for the resolution of the TBTF and cusp-core problems within the CDM paradigm.

Previous hydrodynamical simulations of dwarf galaxies in the WDM paradigm have focused on haloes that are more massive, in a different environment, or have been limited to a single $M_{\rm halo} = 10^{10}\,\mathrm{M}_\odot$ halo and therefore have not explored the range of SFHs that are possible at this mass scale (Herpich et al. 2014; Colín et al. 2015; Governato et al. 2015; González-Samaniego, Avila-Reese & Colín 2016; Lovell et al. 2017b). Additionally, previous works have used other galaxy formation prescriptions which can result in different galaxy properties at this mass scale, as discussed above for CDM. A goal of this paper is to explore that galaxy formation threshold in a resonantly-produced sterile neutrino WDM

model where the halo mass is also near the half-mode mass (see Section 2) where free-streaming effects are significant. We seek to answer several questions: How does the central density profile respond when both stellar feedback and free-streaming effects are prevalent? What happens to the SFHs in galaxies that sit at both dark matter and galaxy formation thresholds? Can galaxy properties in dwarf galaxies that reside in dark matter haloes where dark matter effects are so prevalent be used to discriminate between dark matter models?

To address these questions, we resimulate 8 of the 12 dwarf galaxies from Fitts et al. (2017) in a resonantly-produced sterile neutrino cosmology in order to make a one-to-one comparison between CDM and WDM effects in our simulations. All of our simulations use the GIZMO code[1] (Hopkins et al. 2014; Hopkins 2017) and the Feedback in Realistic Environments (FIRE)-2 galaxy formation and feedback model (Hopkins et al. 2018).[2] We provide an overview of our simulations and the sterile neutrino model in Section 2. In Section 3 we present our results for the WDM halo properties and their central galaxies in a WDM cosmology. We discuss these results in Section 4 and conclude in Section 5.

2 SIMULATION DETAILS AND WDM STRUCTURE FORMATION THEORY

In CDM, structure formation proceeds hierarchically: larger haloes are built up through the merging of smaller dark matter haloes. As a result of free-streaming effects, WDM structure formation may proceed differently depending on the WDM model parametrization and the halo mass scale under consideration (Barkana et al. 2001; Bode et al. 2001; Smith & Markovic 2011; Schneider et al. 2012). WDM models define two wavenumbers that are relevant for structure formation, the free-streaming scale ($k_{\rm fs}$) and the half-mode scale ($k_{1/2}$). Below the free-streaming scale, primordial perturbations are erased by the time structure formation begins, wiping out the seeds of low-mass dark matter haloes. The half-mode scale is defined implicitly as $T_{\rm rel}(k_{1/2}) = \sqrt{P_{\rm WDM}/P_{\rm CDM}} = 0.5$, where $T_{\rm rel}$ is the 'relative' transfer function that describes the suppression of the WDM model relative to CDM. WDM haloes with masses above the half-mode mass,

$$M_{1/2} = \frac{4\pi}{3}\left(\frac{\pi}{k_{1/2}}\right)^3 \bar{\rho}\,, \tag{1}$$

build-up in a similar hierarchical fashion as in CDM (Smith & Markovic 2011; Schneider et al. 2012). Below the half-mode mass but above the free-streaming mass,

$$M_{\rm fs} = \frac{4\pi}{3}\left(\frac{\pi}{k_{\rm fs}}\right)^3 \bar{\rho}\,, \tag{2}$$

free-streaming effects are significant and the mass assembly history of WDM haloes may be far different than their CDM counterparts: hierarchical formation may break down and WDM haloes may form through monolithic collapse (Avila-Reese et al. 2001; Barkana et al. 2001; Bode et al. 2001; Smith & Markovic 2011; Angulo, Hahn & Abel 2013; Schneider, Smith & Reed 2013)

This work considers sterile neutrinos that are resonantly produced in the presence of a large lepton asymmetry (Shi & Fuller 1999); the resulting non-thermal momentum distribution depends on a combination of the mixing angle between sterile and active neutrinos, the cosmological lepton number, and the sterile neutrino mass. The model parameter choices set the momentum distribution and defines the shape of the 'relative' transfer function. We calculate the exact transfer function using the formulation of Venumadhav et al. (2016) for an $m_\nu = 7.1$ keV sterile neutrino and model parameters that are consistent with the observed 3.55 keV X-ray line. Our model choice is then defined by a mixing angle of $\sin^2(2\theta) = 2.9 \times 10^{-11}$ (hereafter, S229). As discussed in Bozek et al. (2016), the thermal root mean square velocity of our model is a small fraction of the typical Zel'dovich velocities at the start of the simulation. As the contribution is negligible, we do not include the relic velocity distribution of the WDM in the initial conditions of our simulations.

The S229 model is selected for free-streaming behaviour that addresses both the Missing Satellites and TBTF problems while remaining consistent with the current count of galaxies in the Local Group (Bozek et al. 2016; Horiuchi et al. 2016). The TBTF problem is not solved completely by the free-streaming component of the model, which motivates studying this model in full hydrodynamical simulations. The half-mode mass of the S229 model, $M_{1/2} = 1.2 \times 10^9\,{\rm M}_\odot$, is comparable with a thermal WDM model with $m_{\rm THM} = 2$ keV, however the S229 model has a smaller free-streaming mass of $M_{\rm fs} \sim 2.5 \times 10^5\,{\rm M}_\odot$ because of its 'colder' intrinsic velocity (Venumadhav et al. 2016) distribution.[3] Given that the final virial mass of the haloes we consider here is only a factor of ∼10 larger than the half-mode mass, the mass assembly histories of WDM haloes will likely differ somewhat from their CDM counterparts: at early times, the progenitor haloes will have low enough masses, free-streaming effects are relevant (i.e. $M_{\rm prog} \lesssim M_{1/2}$; see Schneider et al. 2012). Previous studies of galaxy formation in comparable WDM models found CDM and WDM galaxy properties to be similar (Herpich et al. 2014; Colín et al. 2015; Lovell et al. 2017a). However, those studies were in more massive haloes, different large-scale environments, or focused on a single galaxy, motivating our study using a suite of galaxies.

Numerical simulations of WDM models suffer from numerical artefacts induced by discreteness noise (Wang & White 2007); this effect occurs on scales with essentially no power in the initial conditions and is therefore limited to mass scales below $M_{\rm lim} = 10.1\,\bar{\rho}\,d\,k_{\rm peak}^{-2}$ (Wang & White 2007). Our $z = 0$ haloes should be insensitive to these numerical effects, as they have masses significantly in excess of $M_{\rm lim} = 2.4 \times 10^7\,{\rm M}_\odot$ in our simulations (where we have followed Lovell et al. (2014) and multiplied the Wang & White (2007) definition by $\kappa = 0.5$). We note that while we do not remove artificial haloes from our analysis, contamination from spurious haloes does not appear to impact the assembly histories of our dark matter haloes or their central galaxies: the main features of our WDM simulations track CDM histories, as detailed below.

We selected eight haloes from the CDM simulation suite of Fitts et al. (2017) to be resimulated in WDM; we simulated DMO and hydrodynamical versions in each case. The haloes were selected for zoom-in simulations from a parent box of $L = 25\,h^{-1}$ Mpc; the targeted halo was required to be isolated from any more massive halo by at least three virial radii (of the more massive halo), allowing us to study the formation of the haloes and the galaxies independent

[1] A public version of GIZMO is available at http://www.tapir.caltech.edu/phopkins/Site/GIZMO.html

[2] FIRE project website: http://fire.northwestern.edu

[3] We will refer to models with smaller (larger) free-streaming lengths relative to S229 as 'colder' ('warmer') models

of environmental effects. Additional details on halo selection can be found in Fitts et al. (2017).

Our simulations use the FIRE-2 galaxy formation and feedback model with identical physics and model parameters as those in Hopkins et al. (2018). We briefly summarize the FIRE-2 model here; a more detailed description can be found in Hopkins et al. (2018). Gas cooling is computed for ionized, atomic, and molecular gas from $T \sim 10$–10^{10}K and includes metal-line cooling for 11 elements. Heating and ionization is incorporated from (1) local stellar sources and (2) a redshift-dependent, spatially uniform meta-galactic UV background (updated from Faucher-Giguère et al. 2009).[4] Star formation proceeds in locally self-gravitating, dense, self-shielding molecular, Jeans-unstable gas. Feedback sources have inputs taken from stellar evolution models and include: SNe I and II, stellar mass-loss from O/B-star and AGB-winds, and multi-wavelength photo-heating and radiation pressure. The gas particle mass is $500\,\mathrm{M}_\odot$ and the dark matter particle mass is $2500\,\mathrm{M}_\odot$, with physical force resolution of $h_\mathrm{b} = 2\,\mathrm{pc}$ and $\epsilon_\mathrm{DM} = 35\,\mathrm{pc}$. Simulations are run in a WMAP7 cosmology: $\Omega_\mathrm{m} = 0.266$, $\sigma_8 = 0.801$, $\Omega_\Lambda = 0.734$, $n_\mathrm{s} = 0.963$, and $h = 0.71$ (Larson et al. 2011). Initial conditions for the simulations are created with the MUSIC code (Hahn & Abel 2011).

We use the Amiga Halo Finder (AHF; Knollmann & Knebe 2009) to identify self-bound dark matter haloes. Following the analysis outlined in Fitts et al. (2017), we use the iterative 'shrinking spheres' centring routine (Power et al. 2003) to identify halo centres. For DMO simulations, we correct particle masses using $m_\mathrm{p} \rightarrow (1 - f_\mathrm{b})\,m_\mathrm{p}$, where $f_\mathrm{b} = \Omega_\mathrm{b}/\Omega_\mathrm{m}$ is the cosmic baryon fraction, which effectively mimics maximal baryonic mass-loss for DMO runs. All virial quantities are defined according to Bryan & Norman (1998). The virial overdensity relative to ρ_c is $\Delta_\mathrm{c} = 96.5$ for our chosen cosmology. Consistent with Fitts et al. (2017), we define the stellar mass of a galaxy as $M_\star(< 0.1\,R_\mathrm{vir})$.

3 RESULTS

3.1 WDM halo properties and assembly in DMO simulations

This section focuses on the assembly histories and halo properties of WDM haloes in the DMO simulations. We will highlight how WDM structure formation proceeds differently than in CDM and identify dark matter halo features that will impact galaxy formation when baryons are added later in the hydrodynamical runs. The global properties of the WDM haloes are detailed in Table 1.

Fig. 1 shows the assembly histories of the WDM haloes (and their CDM counterparts) in the DMO simulations. The WDM and CDM haloes have similar final masses of $M(z = 0) \approx 10^{10}\,\mathrm{M}_\odot$, but WDM haloes collapse later and the first haloes to form are much more massive in WDM than in CDM. We define the collapse mass as the halo mass at the snapshot time when the halo is first identified by AHF as a bound object with a minimum of 200 dark matter particles, corresponding to a mass above $M_\mathrm{vir} = 5 \times 10^5\,\mathrm{M}_\odot$. The collapse masses of the WDM haloes all lie between the half-mode mass and free-streaming mass of $M_\mathrm{fs} \sim 2.5 \times 10^5\,\mathrm{M}_\odot$ and $M_{1/2} = 1.2 \times 10^9\,\mathrm{M}_\odot$. The assembly histories of the WDM haloes quickly catch up to their CDM counterparts by $z \sim 3$–4 and subsequently track the CDM halo growth. The inflection point in the assembly history marks the end of the rapid collapse phase (Wechsler et al. 2002; Zhao et al. 2003), which both WDM and CDM haloes exit at similar times despite very different initial halo collapse times. The larger collapse mass of the WDM halo allows for a rapid collapse period that is shorter than in CDM. The colour of the curves in Fig. 1 correspond to the stellar mass of the galaxy from the hydrodynamical simulation of that halo (see Table 2). The DMO simulation halo masses at the end of the rapid collapse phase ($z \sim 3$–4) in both WDM and CDM models are correlated with the stellar mass of the galaxies that will form in those haloes in the hydrodynamical simulations.

Free-streaming smooths density fluctuations on small scales in WDM, resulting in later collapse of WDM haloes when the background density of the Universe is lower; this results in a reduced central density relative to CDM. The top panel of Fig. 2 shows the density profiles of the WDM haloes at $z = 0$ for the DMO simulations; the range of their CDM counterparts is shown in the grey-shaded region. The overall reduction in the central density can be seen in the shift of the WDM curves downward from the grey band that extends out to $r \sim 20\,\mathrm{kpc}$; the concentrations of the WDM haloes are also reduced, as the peak of $\rho\,r^2$ shifts to larger values relative to the CDM case. The colour of the curves in Fig. 2 are the same as in Fig. 1. The central density of the WDM haloes in the DMO simulations are correlated with stellar mass of the galaxies that will form in the corresponding hydrodynamical simulation haloes, as was shown in Fitts et al. (2017) for CDM. The denser the WDM halo in the DMO simulation the larger the galaxy stellar mass will be in a hydrodynamical simulation.

The ratio of the density profiles (WDM to CDM) is shown in the bottom panel of Fig. 2. At $r = 500\,\mathrm{pc}$,[5] the density ratio of WDM to CDM haloes is 0.6–0.85, which is very similar to the value found by Bozek et al. (2016) for field haloes at this mass scale in the vicinity of a simulated Local Group analogue.

Moving out from the centre of the haloes, the density ratio remains below 0.8 for the central few kiloparsecs and below unity out to $r \sim 10$–$30\,\mathrm{kpc}$ from the halo centres. Most haloes have a relatively constant WDM to CDM density ratio out to $r \sim 10\,\mathrm{kpc}$. Halo m10m is the one exception: it has a ratio that rises towards the centre at $r < 1\,\mathrm{kpc}$, which is the result of a late-time minor merger in the WDM run.

3.2 Dark matter halo – stellar mass connection

The previous section focused on the WDM halo properties from DMO simulations. In this section, we consider the WDM haloes from the hydrodynamical simulations to explore the connection between the dark matter halo properties and the central galaxy stellar mass. The global properties of our simulated galaxies, including the central galaxy stellar mass, are listed in Table 2.

Fig. 3 shows the WDM and CDM haloes' V_max (as coloured lines and a grey-shaded region, respectively) as a function of time in the hydrodynamical simulations. The peak V_max value for each WDM halo is lower than its CDM counterpart, which corresponds to the reduction of the central density of the WDM haloes shown in Fig. 2 for the DMO simulations. The inflection point in the evolution of V_max with time between $t = 1$–$4\,\mathrm{Gyr}$ ($z_\mathrm{f} = 5.8$–1.7)

[4]This UV background model is available at http://galaxies.northwestern.edu/uvb

[5]We make several comparisons of between WDM and CDM at $r = 500\,\mathrm{pc}$ throughout the paper. This value was chosen to represent a fixed point near the centre of the halo that is close to the average half-light radius of galaxies in WDM haloes and is roughly $2\,r_\mathrm{conv}$. The convergence radius for each halo is determined by the Power et al. (2003) criterion. We select the largest value of $r_\mathrm{conv,max} = 265\,\mathrm{pc}$ as the minimum radius for all haloes.

Table 1. Global properties of WDM haloes at $z = 0$, including comparisons with their CDM counterparts, for the hydrodynamical simulations. *Column 1*: Halo name; *Column 2*: maximum amplitude of rotation curve; *Column 3*: virial mass; *Column 4*: formation redshift; *Column 5*: WDM–CDM virial mass ratio; *Column 6*: WDM–CDM central density ratio; *Column 7*: Einasto concentration parameter for WDM haloes; *Column 8*: Einasto concentration parameter for CDM haloes.

Halo	$V_{\rm max}$ [km s^{-1}]	$M_{\rm vir}$ [10^{10} M$_\odot$]	$z_{\rm f}$	$M_{\rm vir,WDM}/M_{\rm vir,CDM}$	$\rho_{\rm WDM}/\rho_{\rm CDM}$(500 pc)	$c_{\rm Ein,WDM}$	$c_{\rm Ein,CDM}$
m10b	27.59	0.74	1.24	0.81	0.56	9.6	13.7
m10c	26.36	0.67	2.89	0.77	0.80	9.4	10.9
m10d	28.40	0.70	5.37	0.84	0.68	11.7	14.3
m10e	28.23	0.85	2.12	0.85	0.79	8.0	9.4
m10f	31.23	0.76	5.37	0.90	0.54	11.4	17.0
m10h	35.34	1.10	4.16	0.88	0.77	12.5	14.4
m10k	36.12	1.10	3.77	0.97	0.92	11.4	12.6
m10m	35.73	1.08	5.59	0.96	0.94	13.6	15.2

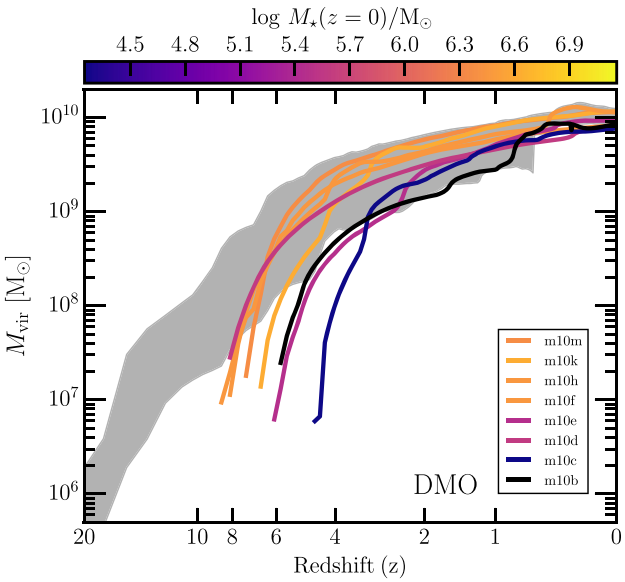

Figure 1. The assembly history of the WDM haloes (curves) in the DMO simulations. The range of assembly histories for the CDM counterparts of the WDM haloes are shown by the grey band. WDM haloes collapse later and collapse with a larger mass than their CDM counterparts. The colour of the curves corresponds to the $z = 0$ stellar mass of the galaxy that resides in each halo in the corresponding hydrodynamical simulations (described further in Section 3.2). $M_\star(z = 0)$ is correlated with the halo mass at the end of the rapid collapse phase.

marks the point where the central halo potential, as measured by $V_{\rm max}$, is set. Beyond this point, $V_{\rm max}$ is relatively constant for each halo, indicating that subsequent mass accretion does not add to the central gravitational potential. The inflection point in $V_{\rm max}$ also coincides with the end of the rapid collapse phase of the halo's mass assembly history as shown in Fig. 1 for the DMO simulations. The WDM haloes are therefore being built up inside-out, similar to CDM haloes (Diemand, Kuhlen & Madau 2007), where the inner halo forms first during the rapid collapse phase and the outer layers are added as the halo accretes additional mass. This indicates that WDM haloes are growing hierarchically at this mass scale, albeit with a near monolithic inner halo assembly history that differs from CDM.

The colour of the curves in Fig. 3 are the same as in the previous two figures. As was shown by Fitts et al. (2017) for CDM, the peak $V_{\rm max}$ value for each WDM halo is correlated with $M_\star(z = 0)$ of each galaxy. One halo, m10b (black curves in Figs 1–3), does not form any stars. The right y-axis of Fig. 3 shows the equivalent virial temperature, defined as $kT_{\rm vir} = 0.5\,\mu\,m_{\rm p}V_{\rm max}^2$ (where $\mu = 0.59$ for primordial ionized gas and $m_{\rm p}$ is the proton mass), of Halo m10b is below the temperature of reionization heated intergalactic gas ($T \approx 2 \times 10^4$ K) for most of its assembly history preventing the onset of star formation. The SFHs of the WDM galaxies are discussed in detail in Section 3.3.

Fig. 4 shows the relationship between the formation time of the WDM and CDM haloes and the maximum circular velocity at that time. We define the formation time of the halo as the cosmic time where the $V_{\rm max}$ function initially reaches a value of 0.85 $V_{\rm max}(z = 0)$. This choice most accurately selects the critical point in the halo's assembly history where the central halo potential is set. This definition of formation time is similar to that in Diemand et al. (2007); however, our definition is based on the value of $V_{\rm max}$ today instead of the peak value over all time. There are multiple reasons for making this choice. Several haloes in our simulations feature recent mergers that result in temporary spikes in the $V_{\rm max}$ function, as can be seen in Fig. 3, which would artificially shift formation times to later times if the peak $V_{\rm max}$ value was used. Additionally, the haloes in our simulations are isolated and not subject to the same late-time environmental effects of Diemand et al. (2007). Other choices for defining the formation time in the literature that are based on a fraction of the halo's final $M_{\rm vir}$ (Wechsler et al. 2002; Gao, Springel & White 2005) are less appropriate here, as they occur after the physical mass assembly of the halo (Diemand et al. 2007).

The $V_{\rm max}$ value of a WDM halo at the time of formation correlates strongly with the stellar mass of the galaxy at redshift zero, $M_\star(z = 0)$, as shown in the left-hand panel of Fig. 4. The WDM haloes follow a similar $V_{\rm max}(z_{\rm f})$–$M_\star(z = 0)$ relation as the CDM haloes; the decrease in the stellar mass of the galaxies in WDM haloes is in proportion to the reduction in the $V_{\rm max}(z_{\rm f})$. The dashed grey curve in Fig. 4 shows the fit to the $V_{\rm max}(z_{\rm f})$–$M_\star(z = 0)$ relation for both WDM and CDM haloes

$$V_{\rm max}(z_{\rm f}) = 27.5\,{\rm km\,s^{-1}} \left(\frac{M_\star(z=0)}{10^6\,{\rm M_\odot}}\right)^{0.065}. \quad (3)$$

The depth of the central WDM halo potential that is set at the end of the rapid collapse phase determines the final stellar mass of the galaxy, as was found to be the case in CDM by Fitts et al. (2017).

The left-hand panel of Fig. 4 shows that the relation between $V_{\rm max}(z_{\rm f})$ and $M_\star(z = 0)$ holds across WDM and CDM haloes, which is a result of the similar degree of central density suppression in each WDM halo, as shown in the bottom panel of Fig. 2. Each WDM halo features a ∼30 per cent density reduction in the inner 1 kpc relative to CDM independent of the overall density of the CDM

Table 2. Global properties of WDM galaxies at $z = 0$, including comparisons with their CDM counterparts, for hydrodynamical simulations. *Column 1*: Halo name; *Column 2*: Stellar mass of central galaxy [defined as $M_\star(< 0.1\,r_{\rm vir})$]; *Column 3*: WDM–CDM stellar mass ratio; *Column 4*: Gas mass within $r_{\rm vir}$; *Column 5*: Cold H I gas ($T < 10^4$ K) within $0.1\,r_{\rm vir}$ (the mass fraction of H_2 is negligible if present); *Column 6*: 3D stellar half-mass radii; *Column 7*: Star formation rate of central galaxy in last 1 Gyr within $0.1\,r_{\rm vir}$.

Halo	$M_\star$	$M_{\star,\rm WDM}/M_{\star,\rm CDM}$	$M_{\rm gas}$	$M_{\rm H\,I,cold}$	$r_{1/2}$	SFR($t < 1$ Gyr)
	[10^6 M$_\odot$]		[10^7 M$_\odot$]	[10^7 M$_\odot$]	[kpc]	[10^{-5} M$_\odot$ yr^{-1}]
m10b	–	–	11.62	0.07	–	–
m10c	0.02	0.03	10.98	0.08	0.14	0.70
m10d	0.38	0.25	9.18	0.24	0.38	0.89
m10e	0.29	0.15	17.86	1.27	0.34	12.1
m10f	2.76	0.67	11.21	0.78	0.72	5.33
m10h	2.73	0.35	18.91	1.17	0.65	17.8
m10k	4.10	0.39	19.20	0.76	0.81	11.0
m10m	2.22	0.15	9.81	0.0	0.77	0.0

halo. Combined with a slight decrease in the halo concentration, this effect results in a ∼10 per cent reduction in the WDM halo's $V_{\rm max}$ relative to CDM and fits the predicted $V_{\rm max,WDM}$–$V_{\rm max,CDM}$ scaling from Bozek et al. (2016). The $V_{\rm max}(z_{\rm f})$–$M_\star(z = 0)$ and $V_{\rm max,WDM}$–$V_{\rm max,CDM}$ relations could, in principle, be used to predict the WDM halo stellar mass from corresponding CDM simulations. We note that the $V_{\rm max}(z_{\rm f})$–$M_\star(z = 0)$ relation has been determined for haloes at 10^{10} M$_\odot$ and may not hold at higher masses. Another caveat to this prescription are cases such as Halo m10b that does not form stars in WDM. We explore WDM galaxy formation histories in the following sections.

Fig. 5 shows the line-of-sight velocity dispersion of stars within the stellar half-mass radius in the simulated WDM and CDM galaxies. The line-of-sight velocities are determined by randomly distributing 100 virtual observers around each galaxy and measuring each star's velocity along each observer's line of sight. The measured velocity dispersions of isolated and Milky Way dwarf galaxies from Kirby et al. (2014) are also shown in Fig. 5. The kinematic properties of our simulated dwarf galaxies in both WDM and CDM agree well with the range of velocity dispersions observed in nearby dwarf galaxies. The agreement between observed and simulated dwarf galaxy kinematic properties indicates that $V_{\rm max}(z_{\rm f})$–$M_\star(z = 0)$ relation for simulated galaxies should also hold for Local Group dwarfs.

3.3 Galaxy properties in WDM

Some properties of the WDM galaxies, including gas and stellar content, are listed in Table 2. Many of these are broadly consistent with their CDM counterparts; certain properties can differ notably, however, and these cases are discussed below. The WDM galaxies simulated here are all dispersion-supported with no appreciable rotation, similar to FIRE-2 galaxies at this mass scale simulated in CDM and consistent with observations (Fitts et al. 2017; Wheeler et al. 2017)

The left-hand panel in Fig. 6 shows the stellar mass growth histories of the galaxies residing in the main progenitor branches of the WDM haloes. The stellar mass growth histories are varied in detail and span a wider range of assembly tracks than their CDM counterparts, as can be seen by comparing the coloured lines (WDM) to the grey band. In the previous section, we established the halo's $V_{\rm max}$ at the time of formation as the main determinant of $M_\star$. Dividing the WDM galaxies into two groups, high stellar mass ($M_\star \geq 10^6$ M$_\odot$) and low stellar mass ($M_\star < 10^6$ M$_\odot$), we see that the high stellar mass galaxies all have a $V_{\rm max}(z_{\rm f}) > 25$ km s^{-1} while lower $V_{\rm max}(z_{\rm f})$ haloes form significantly fewer stars or do not form stars at all.

Generally, the high $M_\star$ galaxies of our suite reside in haloes that collapse earlier ($z_{\rm c} > 6$), have earlier formation times ($z_{\rm f} > 3.5$), and begin to form stars early on in their assembly history ($z_{\star,\rm i} > 4$). Earlier formation allows this subset of WDM haloes to build a reservoir of gas that can drive sustained star formation. However, these parameters are not exactly correlated with the final stellar mass of the galaxy. For example, the most massive WDM galaxy (Halo m10k) collapses last, has the latest formation time, and does not begin to form stars until $z \sim 4.5$ (last amongst the larger stellar mass galaxy group). The onset of star formation in Halo m10k begins even later than in Halo m10d ($z \sim 7$), which forms one-tenth as many stars.

The right-hand panel of Fig. 6 shows the SFHs as they would be constructed observationally via the method of 'stellar archaeology'. Archaeological SFHs are constructed by determining the fraction of stars present in the halo at $z = 0$ that were formed at an earlier time. Qualitatively, the SFHs of the massive WDM galaxies (as well as Halo m10d from the low-mass group) are comparable with those of CDM galaxies in Fitts et al. (2017, shown in grey in the right-hand panel of Fig. 6) and observed dwarf galaxies in the field (Cole et al. 2014; Skillman et al. 2014), demonstrating either sustained star formation over their lifetimes or quenching following an early period of star formation. The WDM galaxies that are actively star forming (see Table 2) have specific star formation rates that range from $10^{-10.7}$ to $10^{-9.4}$ yr^{-1}, consistent with our simulated CDM galaxies.

However, the SFHs of individual haloes in CDM and WDM can be very different. For example, in WDM, Halo m10m has a strong feedback event at $z \sim 3$ that drives out all cold interstellar medium (ISM) gas, heats the circumgalactic medium[6] to temperatures above the halo virial temperature, and prevents gas cooling on to the galaxy until $z \sim 0$. In CDM, Halo m10m does not quench, but instead has a steady growth over its lifetime and is the most massive galaxy in our CDM galaxy sample. Stemming from the delay in WDM structure formation, the start of star formation for all our WDM galaxies is delayed relative to CDM, as was noted by Governato et al. (2015) for a halo at this mass scale simulated with a different set of galaxy formation models. We find that the delay in the onset

[6]We define the ISM to be the gas with $r \leq 0.1R_{\rm vir}$ and the circumgalactic medium to be gas with $r_{\rm ISM} < r \leq R_{\rm vir}$.

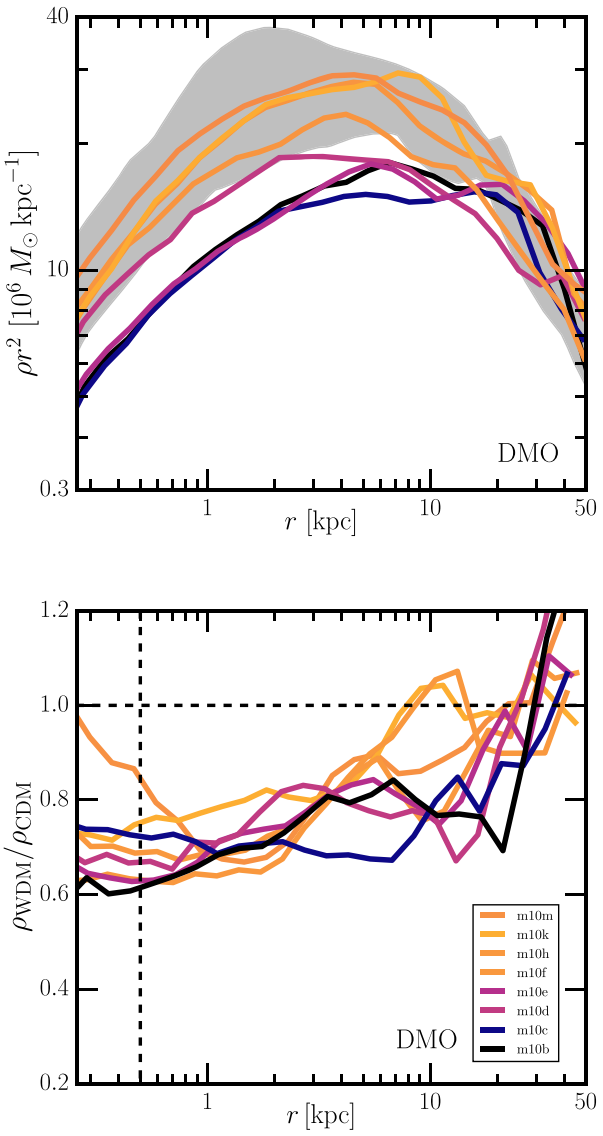

Figure 2. *Top Panel:* The density profiles of the WDM haloes (coloured curves) from the DMO simulations and their CDM (DMO) counterparts (grey band). The line colours are the same as in Fig. 1. The downward shift of the curves relative to the grey band indicates the WDM haloes are less dense than their CDM counterparts out to 10 kpc, where the curves and grey band overlap. To first order, the stellar mass of the galaxy at $z = 0$ correlates with the central density of the halo, i.e. denser DMO haloes have brighter galaxies in their hydrodynamical counterparts. *Bottom Panel:* The ratio of WDM to CDM density profiles from the top panel. There is a 15–40 per cent reduction in the central density of WDM haloes relative to CDM at 500 pc (dashed vertical line) and the ratios remain below 0.8 out to a few kpc for all WDM haloes; since the figure compares DMO profiles, this reduction is entirely attributable to the effects of free-streaming in WDM. The up-sloping density profile ratio for $r < 1$ kpc for Halo m10m is likely due to a late merger. The degree of the WDM halo density reduction in DMO simulations is independent of the halo's central density.

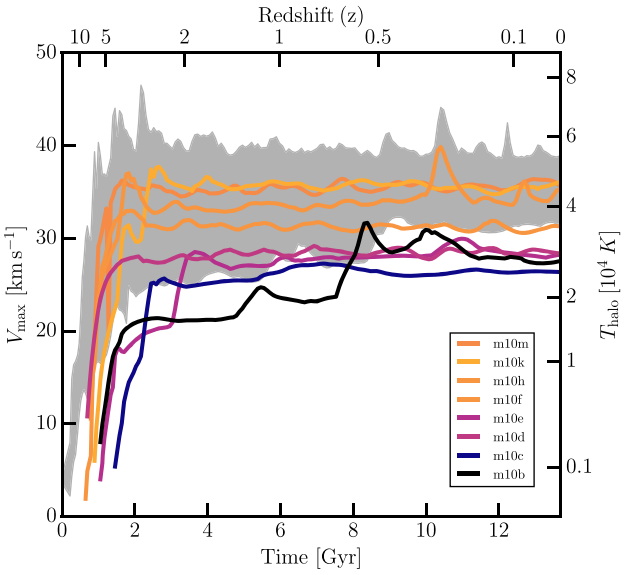

Figure 3. $V_{\rm max}$ as a function of time for the WDM haloes (curves) and their CDM counterparts (grey band) for the hydrodynamical simulations. The equivalent virial temperature, $T_{\rm vir}$, is given on the right axis. Following the period of rapid collapse, the peak $V_{\rm max}$ sets in at $t_{\rm f} \sim 1$–4 Gyr ($z_{\rm f} = 5.8$–1.7) and remains mostly constant to $z = 0$, with the exception of a late-time major merger for Halo m10b (black). The line colour is the same as in previous figures and indicates that $M_\star(z = 0)$ is closely connected with the dark matter halo central potential as measured by $V_{\rm max}(z_{\rm f})$. Halo m10b forms no stars, as it has a $T_{\rm vir} < 2 \times 10^4$ K for most of its history. The central potential in WDM is reduced relative to CDM in each case.

of star formation is often as short as ∼0.5 Gyr in our simulations; Governato et al. (2015) found a 1–2 Gyr delay in their WDM simulation, consistent with the range of delays found in our suite.

The galaxies in the low $M_\star$ group are strongly affected by reionization and stellar feedback and form the majority of their stars very early or very late (or not at all). The collapse time, formation time, and subsequently the onset of star formation, strongly affect the diversity of SFHs in low $M_\star$ galaxies shown in Fig. 6. For example, Halo m10d is one of the earliest collapsing haloes in WDM that has an early onset of star formation before quenching; its SFH in WDM qualitatively resembles the CDM version, where it forms all of its stars prior to $z = 5$ and remains quenched until $z = 0$. In WDM, however, the quenching is transient: it forms over 80 per cent of its stars before quenching at $z \sim 3$ and subsequently restarting star formation at $z \sim 0.5$. The quenching event of WDM Halo m10d is less extreme than in CDM (or compared with WDM Halo m10m) owing to a smaller initial star formation rate that produces less energetic feedback. Unlike Halo m10m, Halo m10d is immediately able to re-accrete warm gas (defined here as 10^4 K $< T < 10^5$ K), allowing sufficient time to restart star formation by $z = 0.5$.

The SFHs of the three remaining WDM haloes (Halo m10b, m10c, and m10e) are significantly different than their CDM counterparts; Halo m10b is an extreme example, as it does not form any stars in WDM by $z = 0$. Reionization heating suppresses additional accretion of intergalactic gas for Haloes m10b and m10c in WDM until $z \sim 2$, when the UV background weakens. Halo M10c has a virial temperature at $z_{\rm f}$ that is slightly larger than the temperature to which reionization heats intergalactic gas ($T \approx 2 \times 10^4$ K), resulting in an appreciable reservoir of gas following halo collapse and the ability to accrete gas after $z \sim 2$. Halo m10b, on the other hand, has $T_{\rm vir} < 2 \times 10^4$ K for most of its assembly history; it is only at $z \sim 0.5$, when it experiences a major merger, that it is able to accrete additional warm gas that begins cooling at $z \sim 0.2$. With this late-time build-up of cold gas, there is the possibility that Halo m10b will form stars in the future. In the CDM simulation, Halo

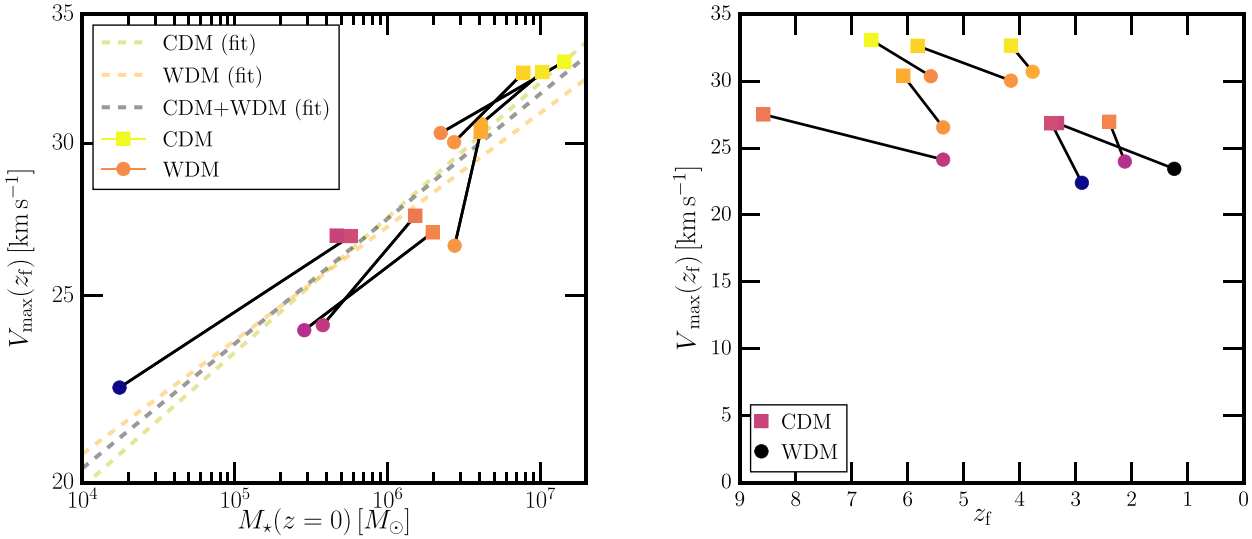

Figure 4. *Left-hand Panel:* $V_{\rm max}(z_{\rm f})$ at the time of halo formation correlates with the stellar mass of the galaxy at $z = 0$. WDM and CDM halo counterparts are connected by black segments. WDM haloes (circles) have a smaller $V_{\rm max}(z_{\rm f})$ than their CDM counterparts (squares) and, as a result, a lower stellar mass that moves the galaxy along the $V_{\rm max}(z_{\rm f})$–$M_\star(z = 0)$ relation. The three $V_{\rm max}(z_{\rm f})$–$M_\star(z = 0)$ fits shown for WDM haloes only (dashed orange), CDM haloes only (dashed yellow), and WDM and CDM haloes together (dashed grey) are similar. *Right-hand Panel:* The $V_{\rm max}(z_{\rm f})$ as a function of formation time. Haloes form later and with a $V_{\rm max}$ that is reduced by ∼10 per cent in WDM relative to CDM. $V_{\rm max}(z_{\rm f})$ and $z_{\rm f}$ are not strongly correlated. The colour scheme is the same as is used in previous figures.

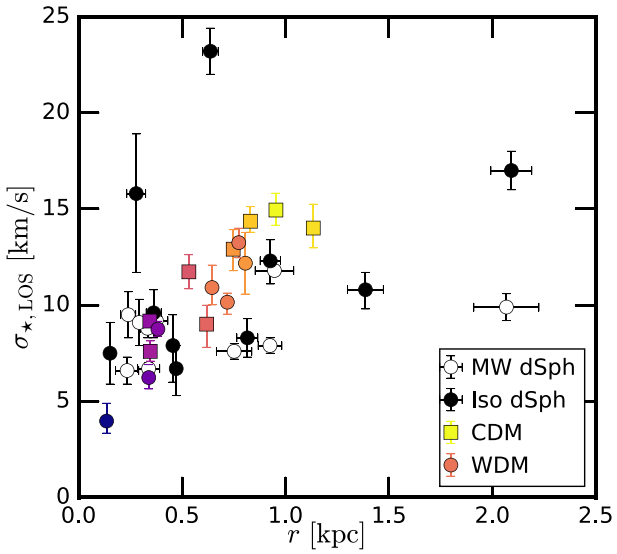

Figure 5. The stellar line-of-sight velocity dispersion at the 3D stellar half-mass radius for the simulated WDM (circles) and CDM (square) galaxies. The error bars mark the 16th and 84th percentiles. The stellar line-of-sight velocities are determined by randomly distributing 100 virtual observers around each simulated galaxy. The solid (open) black points are the measured velocity dispersions at the 3D de-projected half-light radii of the isolated (Milky Way) dwarf galaxies from Kirby et al. (2014). The simulated dwarf galaxies lie within the range of observed galaxy properties.

m10b has a qualitatively similar halo assembly history, but a larger $V_{\rm max}$ at all times, resulting in multiple star formation episodes and multiple galaxy mergers (Fitts et al. 2018). In the larger CDM halo suite of Fitts et al. (2017), there is one halo (m10a) that does not form any stars; that halo has a similarly suppressed $T_{\rm vir}$(z) as the WDM version Halo m10b. A major difference between the 'dark' halo in CDM and WDM is the absence of cold gas in the CDM case compared to a significant amount of cold gas in WDM.

Finally, we consider Halo m10e, which has a larger gas mass at collapse than Halo m10b and Halo m10c (see Table 2) despite having an early $V_{\rm max}(z)$ evolutionary track that is similar to Halo m10b. As a result, it has an initial burst of star formation immediately following the rapid collapse phase. A merger at $z \sim 2$ raises the halo's $V_{\rm max}$ above the threshold for late-time gas accretion described above, which drives the halo's late star formation epoch. To summarize, all WDM haloes are able to bind warm gas and eventually build sufficient gas densities that enables cooling processes. Earlier collapse more readily allows for the onset of star formation depending on the depth of the central potential and how rapidly the central potential forms.

The right-hand panel of Fig. 6 shows the unique SFHs of WDM Halo m10c and Halo m10e, which build-up the majority of their stellar mass after $z \sim 1$. Leo A is the one observed galaxy with a similar SFH featuring a significant late build-up of stellar mass (Cole et al. 2007). However, Leo A has a larger final stellar mass and a non-zero mass fraction of old stars (Cole et al. 2014), both of which clearly distinguish it from the properties of Halo m10c and Halo m10e. Simulations within the CDM paradigm are able to produce strongly delayed SFHs similar to WDM Haloes m10c and m10e (Ricotti 2009; Shen et al. 2014; Fitts et al. 2017; Wright et al. 2019) but with ancient star formation that better matches Leo A. It is not clear if star formation can be prevented altogether at early times at this mass scale in CDM. The existence of a population of young, gas-rich, actively star-forming ultrafaint dwarfs, including extreme cases like Halo m10c which does not have any stars older than 2 Gyr, makes for a strong prediction of WDM dwarf galaxy formation.

Other WDM galaxy properties follow CDM galaxy scaling relations. Fig. 7 shows the relationship between the stellar half-mass radius of the galaxy, $r_{1/2}$, and the total stellar mass. WDM galaxies are smaller and less massive, but lie along a similar $M_\star$–$r_{1/2}$ relation as their CDM counterparts. For WDM the

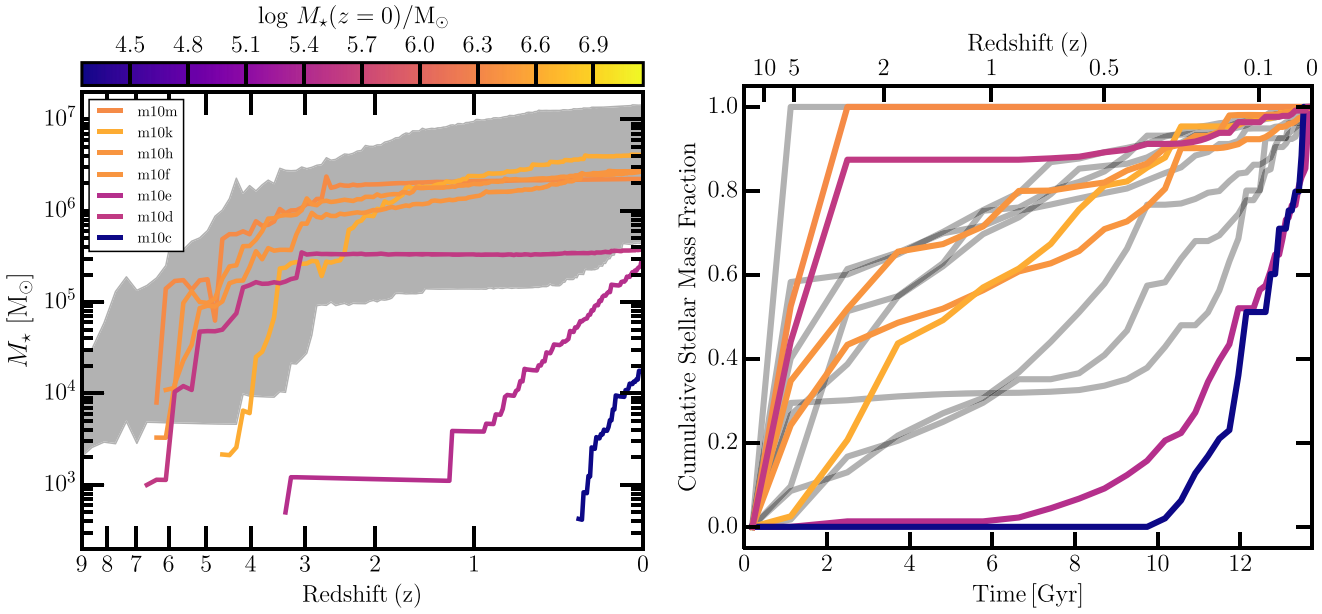

Figure 6. *Left-hand Panel:* The stellar mass assembly histories of the galaxies in WDM haloes (curves) and their CDM counterparts (grey band). The onset of star formation in WDM galaxies is delayed relative to CDM and the $z = 0$ stellar masses are reduced. *Right-hand panel:* The cumulative SFHs of the WDM galaxies (coloured curves) measured in an 'archaeological' manner (by measuring the birth times of stars in the galaxy at $z = 0$). Many of the galaxies have SFHs that are very similar to their CDM counterparts (grey curves), which themselves agree well with observations (Fitts et al. 2017). Two WDM galaxies experience prolonged quenching events. The two least massive galaxies form over 90 per cent of stars after $z = 1$; none of the CDM galaxies exhibit this behaviour.

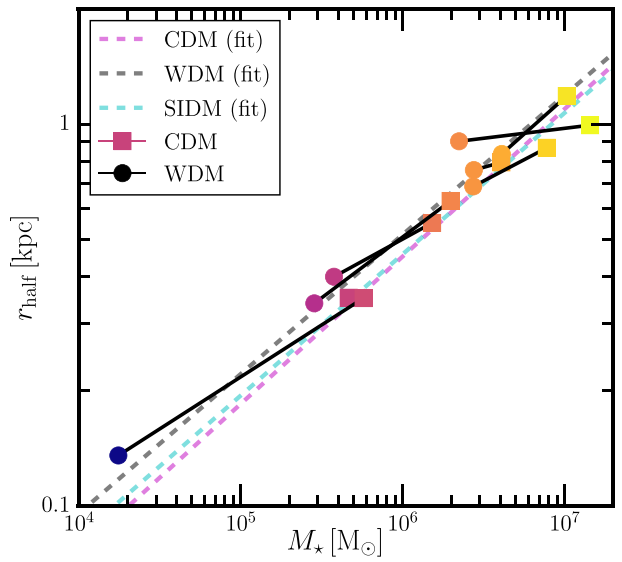

Figure 7. The relationship between the stellar half-mass radius and the stellar mass for the WDM and CDM galaxies at $z = 0$. While the WDM haloes (circles) form fewer stars than their CDM counterparts (squares), the resulting galaxies lie on the same $r_{1/2}$–$M_\star$ relationship. This relationship is also obeyed by self-interacting dark matter simulations of the same haloes as described in Robles et al. (2017) and shown in cyan.

relation is given by $r_{\mathrm{half}} = 0.51\,\mathrm{kpc}\,(M_\star/10^6\,\mathrm{M}_\odot)^{0.365}$. The $M_\star$–$r_{1/2}$ relationship is also very similar self-interacting dark matter (Robles et al. 2017), as is shown in Fig. 7. However, the shapes of the WDM galaxies and their dark matter haloes are triaxial with a similar distribution of axis ratios as their CDM counterparts, which differentiates them from SIDM haloes and galaxies (Robles et al. 2017).

3.4 Feedback effects on WDM halo structure

In this section, we evaluate the impact of stellar feedback on the structure of dark matter haloes. The left-hand panel of Fig. 8 shows the ratio of the density profiles of the WDM haloes from the hydrodynamical simulations compared with density profiles from the DMO simulations. The central density of many WDM haloes in the hydrodynamical simulations are reduced relative to DMO by as much as 45 per cent near the convergence radius of $r_{\mathrm{conv,max}} = 265\,\mathrm{pc}$. As found for $M_{\mathrm{vir}} \approx 10^{10}\,\mathrm{M}_\odot$ haloes in CDM (Fitts et al. 2017), the degree of reduction on the central density profile of WDM haloes roughly correlates with the stellar mass, where low-mass galaxies have little to no effect on their haloes and more massive galaxies show significant central density reductions. This trend and the overall spread in the WDM density profile ratio follows the behaviour of CDM haloes, as indicated by the grey band in the left-hand panel of Fig. 8.

The effects of feedback on the density structure of a galaxy's host halo also depends on the galaxy's SFH. For example, Halo m10m and Halo m10e have similar density ratios (between hydro and DMO in the WDM simulation) at $r = 500\,\mathrm{pc}$ even though Halo m10m hosts a galaxy with 10 times the stellar mass of Halo m10e. At $r = 265\,\mathrm{pc}$, Halo m10e has an additional ∼15 per cent density reduction compared to Halo m10m. The difference in central density profiles of these two haloes can be traced to the very recent star formation of Halo m10e, which forms all of its stars after $z = 1$, while Halo m10m self-quenches at early times; this is consistent with the idea that late-time star formation is important for modifying dark matter halo density profiles (Oñorbe et al. 2015; González-Samaniego et al. 2016; Read et al. 2016). Merger histories can also play a significant role in determining the central density profiles in the hydrodynamical simulations. For example, Halo m10h hosts one of the more massive WDM galaxies and has a

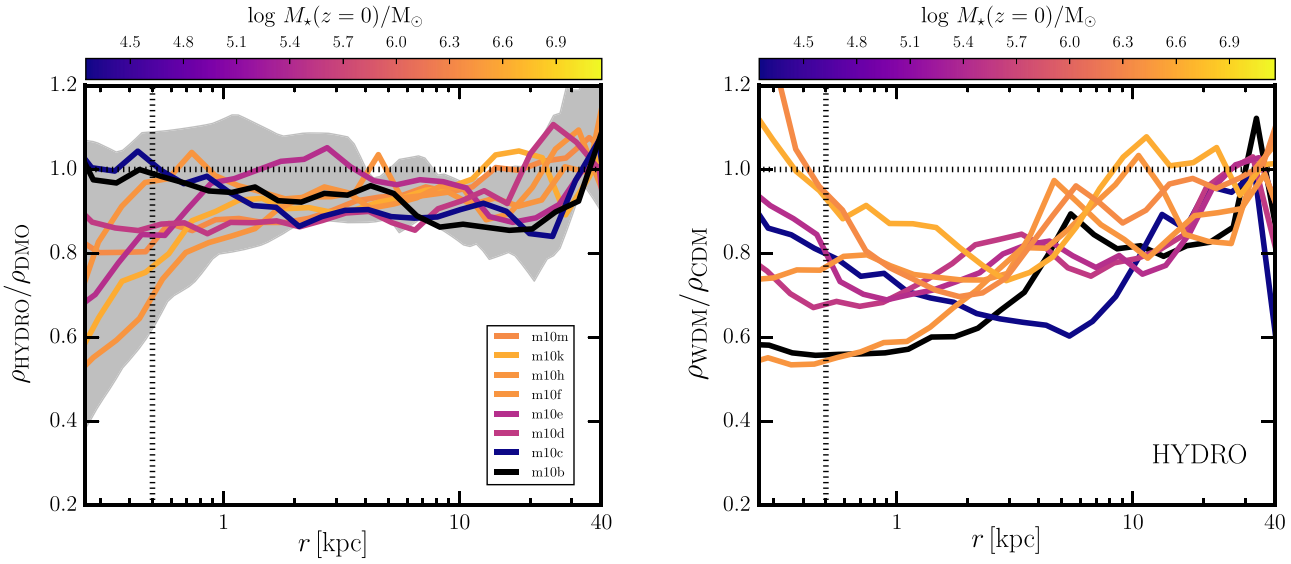

Figure 8. *Left-hand Panel:* The density profile ratios of haloes in the hydrodynamical simulations compared to DMO simulations; line styles are the same as in previous figures. To first order, the stellar mass of the galaxy in WDM and CDM is correlated with the suppression of the central dark matter density from stellar feedback effects. Halo m10h, Halo m10m, and Halo m10e illustrate the second order-effects that require slightly more complicated interpretations. Halo m10h is undergoing a recent merger that raises the density ratio to ∼1 at $r = 500$ pc while maintaining the central density reduction at $r < 500$ pc. Halo m10m (hosting a more massive galaxy) quenches early ($z \sim 3$) and has a similar density ratio at $r = 500$ pc as Halo m10e (which hosts a less massive galaxy), which has formed nearly all of its stars since $z \sim 1$. *Right-hand Panel:* Ratio of density profiles between WDM and CDM haloes from hydrodynamical simulations. There are two galaxies where the CDM halo is less dense than in WDM inside $r \sim 400$ pc (near the numerical convergence radius). All other haloes are less centrally dense in WDM independent of the stellar mass of the galaxy. The dashed vertical line in each panel marks 500 pc; trends in the density at this scale are investigated in Fig. 9.

25 per cent density reduction at $r = 265$ pc, similar to other massive galaxies. However, owing to an ongoing merger of a less massive halo, the density ratio (again, between the hydrodynamic and DMO runs in WDM) at $r \sim 500$ pc is close to unity.

The ratio of density profiles between WDM and CDM from hydrodynamical simulations is shown in the right-hand panel of the Fig. 8. At $r = 500$ pc, all WDM haloes are less dense than their CDM counterparts, and they remain less dense out to $r \gtrsim 10$ kpc. There is no correlation between WDM galaxy stellar mass and the degree of WDM halo central density reduction relative to CDM, as indicated by comparing the colour of the curves in Fig. 8 to the density ratio within the central kpc. For example, Halo m10b has one of the larger central density reductions in WDM relative to CDM in the hydrodynamic simulation even though it does not form any stars in WDM, while Halo m10f hosts one of the more massive WDM galaxies yet has a similar central density profile ratio. Haloes m10k and m10m host the two most massive galaxies in CDM and have density ratios $\rho_{\mathrm{WDM}}/\rho_{\mathrm{CDM}} > 1$ in the inner $r = 400$ pc. These two galaxies have significantly more stellar mass in CDM than in WDM, which results in a greater central density reduction at these radii in CDM. As this is near the convergence radius of our haloes, we restrict further analysis to $r = 500$ pc, where our results are more robust.

Fig. 9 summarizes the effects of the intrinsic reduction to the central density profiles of WDM haloes originating from the delay in halo formation (i.e. coming from the free-streaming length) compared with the effects of feedback in both CDM and WDM hydrodynamical simulations. While galaxies in WDM haloes are less massive and experience fewer significant feedback events than in CDM, the combination of late collapse and baryonic processes leave WDM haloes less dense at $r = 500$ pc in all cases. The two

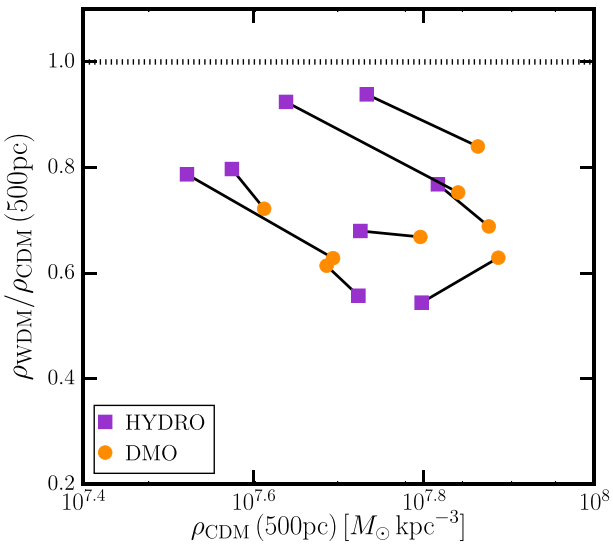

Figure 9. The central density ratio of WDM to CDM in DMO (circles) and hydrodynamical (squares) simulations as a function of the density at 500 pc in CDM simulation (DMO or hydrodynamical, as appropriate). The WDM haloes are less centrally dense than CDM (at 500 pc) in both types of simulation. In hydrodynamical simulations, the two most massive CDM galaxies have density reductions that bring them in close agreement with WDM. In nearly all haloes, stellar feedback processes are more effective in modifying the central dark matter density in CDM than in WDM, which raises the WDM to CDM density ratio for hydrodynamical simulations compared with DMO simulations (in which free-streaming suppresses WDM relative to CDM).

most massive galaxies in our CDM suite have central dark matter halo densities that only exceed their WDM counterparts by ∼5–10 per cent; all other haloes remain ∼20–45 per cent less centrally dense in WDM relative to CDM. The Einasto (1965) concentration parameters for the WDM haloes are also smaller than the CDM haloes (see Table 1).

It is difficult to predict *a priori* whether feedback generally will be more effective at modifying the central density of a CDM halo or its WDM counterpart. On the one hand, the CDM galaxies are typically more massive, meaning they have a larger amount of feedback energy available. On the other hand, WDM haloes form with a reduced central density from free-streaming effects, so it might be possible that even diminished feedback input could have a large effect. In most of our simulated haloes, stellar feedback processes are more effective at modifying the central dark matter density in CDM than they are in WDM (as found in Governato et al. 2015), which raises the ratio of WDM central density relative to CDM in Fig. 9. It therefore appears that the reduced densities of WDM haloes coming from free-streaming do *not* generally make these haloes more susceptible to further density reduction from stellar feedback.

However, this is not always the case. In three haloes (Halo m10b, Halo m10d, and Halo m10f), the ratio decreases or remains flat for differing reasons. Halo m10b has a smaller ratio in the hydrodynamic simulations compared with DMO because the CDM halo in the hydro simulation is denser than it is in DMO, while the central density in the WDM DMO and hydro simulations are identical. The density ratio for Halo m10d is nearly flat; this is because the reduction in the central density profile by stellar feedback is comparable in WDM and CDM (despite the smaller stellar mass and abbreviated SFH in WDM). Halo m10f is the one WDM halo where feedback effects are *more* effective at reducing the central density profile in WDM than in CDM. The extra reduction is modest (∼10 per cent); however, this shows that it is possible to see a larger modification of the density profile in WDM relative to CDM in some cases (as found in González-Samaniego et al. 2016, hereafter GS16). Of all the haloes in our suite, Halo m10f has the most similar stellar mass and average star formation rate in both WDM and CDM cosmologies, which may account for the effectiveness of stellar feedback in modifying its central density in WDM.

4 DISCUSSION

4.1 Predicting trends with WDM halo mass and WDM model parameters

A central motivation of this work is to understand the degree to which the combination of stellar feedback effects and dark matter physics modifies the dark matter distribution in WDM haloes relative to CDM haloes. We have shown that these combined effects make WDM haloes less centrally dense than their CDM counterparts. In this section, we consider extrapolation of those results to different WDM models and different halo masses, as results of the previous sections are specific to $M_{\rm vir}(z = 0) = 10^{10}\,{\rm M}_\odot$ halo mass scale in our simulation suite and the free-streaming scale of the S229 resonantly-produced sterile neutrino WDM model.

Assembly histories of a $M_{\rm halo} = 10^{10}\,{\rm M}_\odot$ in a colder model (e.g. the S220 resonantly-produced sterile neutrino WDM model with $M_{1/2} = 3.1 \times 10^8\,{\rm M}_\odot$ that is discussed in Bozek et al. 2016) would approach CDM assembly histories. S220 dark matter haloes would collapse earlier and form with a larger central density (or equivalently larger $V_{\rm max}(z_{\rm f})$) than the S229 model haloes but with a lower central density than CDM. Given that the slope of the $V_{\rm max}(z_{\rm f})$–$M_\star(z = 0)$ in the left-hand panel of Fig. 4 is similar for CDM and S229, a colder model should follow the same trend with points falling between the S229 and CDM values. The central galaxies would have larger stellar masses, and consequently provide more energy from stellar feedback, but would form initially in a denser dark matter halo than in our WDM case.

An interesting topic for future work is to determine whether the greater amount of stellar feedback in a denser $M_{\rm halo} = 10^{10}\,{\rm M}_\odot$ halo of a colder WDM model will prove more or less efficient at modifying the central dark matter density and result in a smaller or larger $\rho_{\rm WDM}/\rho_{\rm CDM}(r = 500\,{\rm pc})$ ratio. However, we note that Fig. 9 shows that several of our WDM haloes are able to match or exceed the overall reduction in central density compared with CDM despite having smaller stellar masses. It is plausible that there may be a WDM model parametrization (between S229 and CDM) with a maximal reduction in the density profile relative to CDM that exceeds what we find in the right-hand panel of Fig. 8.

While only one ultrafaint dwarf ($M_\star \lesssim 10^5\,{\rm M}_\odot$) in our WDM simulations is formed with a small fraction of ancient (pre-reionization) stars, our results do not preclude the possibility that the S229 WDM model studied here can produce significant numbers of ultrafaint dwarfs with predominantly ancient stellar populations. However, the delay in formation time for the S229 model will limit the fraction of WDM haloes at this mass that will collapse early enough to form old stars (see also Governato et al. 2015). Lower-mass haloes will suffer a longer delay in forming (Bose et al. 2016a), leaving only higher-mass WDM haloes that quench early in their assembly history (similar to CDM models) to additionally host old ultrafaint dwarfs in WDM.

It is difficult to cleanly extrapolate from our results, which are based on galaxies forming in isolated environments, to counts of galaxies in and around the Local Group, where the large-scale overdensity may lead to earlier collapse times and earlier star formation. However, a direct comparison with subahlo $V_{\rm max}$ functions of Local Group analogues does point to difficulties in matching ultrafaint counts in the S229 WDM model if ultrafaints are all predominantly old. Cooler WDM models will have larger fractions of old stellar populations and may not have a similar limitation in their assembly histories. Colder models are also likely to have a population of dark (starless) haloes, similar to CDM (Sawala et al. 2013; Benítez-Llambay et al. 2017; Fitts et al. 2017).

4.2 Implications for reionization in WDM

Half of the WDM dwarf galaxies simulated here do not form any stars before the end of the reionization epoch ($z = 6$). The galaxies that do form stars prior to $z = 6$ have no star formation prior to $z = 7$, however, so they contribute minimally to the ionizing photon background. Their CDM counterparts all form a significant mass of stars prior to the end of the reionization era. The brightest CDM galaxies in our suite have $M_\star \sim 10^6\,{\rm M}_\odot$ at $z = 6$. Extrapolating the stellar mass–UV luminosity relation from Ma et al. (2018), these galaxies will have a UV luminosity of ${\rm M_{UV}} \sim -12$.

In the CDM paradigm, these galaxies make-up a significant fraction of the galaxy population that drives cosmic reionization (e.g. Livermore, Finkelstein & Lotz 2017 and references therein). The galaxy population that sources reionization in WDM is more uncertain. Semi-analytic modelling and abundance matching techniques applied to large-volume cosmological simulations adopting WDM models of comparable warmth to the S229 model demonstrate that reionization can be completed by $z = 6$ while matching

constraints on the epoch of reionization from *Planck* (Schultz et al. 2014; Bose et al. 2016b). However, the abundance of low-mass haloes at high redshift in WDM models is significantly reduced. For example, the S229 model only has about 40 per cent as many haloes with $V_{\rm max}(z = 6) \sim 35\,{\rm km\,s^{-1}}$ relative to CDM (Bozek et al. 2016).

As a result, galaxies in more massive haloes must drive reionization in the WDM paradigm, possibly with a different SFH and ionizing budget than what is predicted for CDM (Bozek et al. 2015; Bose et al. 2016b; Villanueva-Domingo, Gnedin & Mena 2018). Alternatively, other sources such as quasars could be a more important contributor in WDM cosmologies. Including additional sources or considering a different UV background (either in intensity or time) than the one used here could possibly further suppress the late-time SFHs of the low-mass galaxies. Future probes of reionization and counts of galaxies at high redshift provide an important opportunity to constrain WDM models.

4.3 Predicted galaxy populations in WDM

There are features in the galaxy populations that can be used to distinguish between dark matter models. Prior to $z = 7$, the $M_{\rm halo} \approx 10^{10}\,{\rm M_\odot}$ haloes simulated in WDM do not form stars.[7] This implies that it is difficult for this WDM model to account for observations of ultrafaint galaxies in the Milky Way that quench early and have a population entirely made up of old stars (Brown et al. 2014; Weisz et al. 2014).[8] Extrapolating the stellar mass–halo mass relation informed by simulations in the CDM paradigm, ultrafaint galaxies are expected to be hosted in $M_{\rm halo} \approx 10^{9}\,{\rm M_\odot}$ haloes (Moster, Naab & White 2013; Munshi et al. 2013, 2017). As discussed above, isolated ultrafaint galaxies with a significant fraction of stars formed prior to the end of reionization might be hosted by WDM haloes with a range of halo masses, including larger masses ($M_{\rm halo} > 10^{10}\,{\rm M_\odot}$) than the haloes simulated here. This would introduce significant scatter in the low-mass end of the stellar mass–halo mass relation, which has also been proposed in CDM cosmologies (Garrison-Kimmel et al. 2017a).

With a fixed number of $10^{10}\,{\rm M_\odot}$ WDM haloes and a different stellar mass–halo mass relation than in CDM, the faint-end slope of a WDM stellar mass function of field galaxies would be flatter than would be naively expected from halo counts alone predicted by DMO simulations in CDM (Bozek et al. 2016). Counts of faint galaxies detected in future imaging and H I surveys are therefore likely to provide strong constraints on WDM models.

A unique prediction of our suite of WDM galaxies is a population of ultrafaint dwarf galaxies that are extremely young, forming over 80 per cent of their stars in the last 4 Gyr. These galaxies are gas-rich and actively star forming at $z = 0$. Such SFHs are not entirely unlike Leo A (Skillman et al. 2014); however, neither of our late-blooming galaxies has *any* star formation prior to $z \approx 3.5$, unlike Leo A (Cole et al. 2007). There is one galaxy in the CDM sample that forms over 80 per cent of its stars in the last 2 Gyr (Fitts et al. 2017), but it also has a population of ancient ($z \sim 7$) stars, in contrast with the young WDM cases.

Both dark matter models predict haloes that do not form any stars, so it is possible that a CDM model could produce a similarly young ultrafaint dwarf. In that case, the central density profile of the dwarf could help to constrain which type of dark matter halo it resides in, as it would be at least 20 per cent denser in CDM than in WDM according to Fig. 9. Further, if similarly young galaxies form in CDM, they would likely be less abundant. The discovery of a population of galaxies with entirely young stars residing in haloes at this mass scale would therefore strongly disfavour CDM and favour a WDM model.

4.4 Comparison with previous results

Our results complement and extend previous hydrodynamical simulations of isolated WDM dwarf galaxies (Herpich et al. 2014; Governato et al. 2015; Colín et al. 2015; GS16). We do find a few notable differences, however. Unlike all previous WDM studies at this mass scale, our simulated dwarfs are dispersion-supported and do not feature stellar discs; this is consistent with FIRE-based CDM results. Further, our larger suite of WDM galaxies has a broader range of SFHs than previous studies. Finally, the impact of stellar feedback on a galaxy's central density in our simulations is intermediate to that of GS16, who found WDM galaxies more effective at modifying their central density than in CDM, and Governato et al. (2015), who found the opposite (albeit for a single galaxy).

Unlike GS16 (but similar to Governato et al. 2015), we find that the reduction in a galaxy's central density is correlated with its stellar mass, with higher $M_\star$ systems more effective in modifying their central densities. However, as found by GS16, we show the combination of stellar feedback and free-streaming effects can be more effective at reducing the central density in WDM than in CDM, albeit only in certain cases and at a lower level than reported in GS16. These differences highlight the importance of studying galaxy formation in WDM cosmologies with varying star formation prescriptions more thoroughly.

5 CONCLUSIONS

In this paper, we have presented simulations of eight isolated dwarf galaxies with a halo mass of $M_{\rm halo} = 10^{10}\,{\rm M_\odot}$ in WDM using the FIRE-2 galaxy formation model. The underlying dark matter particle model is a resonantly-produced sterile neutrino with a mass of $m_{\rm s} = 7.1\,{\rm keV}$ and a mixing angle of $\sin^2(2\theta) = 2.9 \times 10^{-11}$. This model was selected to (1) provide free-streaming effects that are at the warm edge of what is allowed based on satellite galaxy counts and large-scale structure constraints and (2) account for the origin of possible detections of an X-ray line at 3.55 keV in galaxy and galaxy cluster observations. These isolated dwarfs were also studied in CDM in Fitts et al. (2017). A summary of our main results is as follows:

(i) WDM haloes collapse later and with a larger initial mass than their CDM counterparts. This results in a shorter, near-monolithic period of initial collapse that allows WDM haloes to catch up to their CDM counterparts in the halo assembly process. Following this rapid collapse phase, the central halo potential (as measured by the halo $V_{\rm max}$) is set at a similar cosmic period of $t \sim 2$–$4\,{\rm Gyr}$

[7] The UV background model used in our simulations results in a reionization redshift of $z \approx 10$, which is slightly earlier than found by the Planck Collaboration XIII 2016. This may impact the onset of star formation in our simulated WDM galaxies. We note, however, that the Planck result is a mean reionization redshift, and overdense regions such as the Local Group may have reionized somewhat earlier (e.g. Lunnan et al. 2012).

[8] This statement assumes that the truncation in the ultrafaint dwarf SFH is set by reionization feedback effects. Recent observations of M31 ultrafaint dwarf galaxies have found extended SFHs, implying that the Milky Way utlrafaint satellite SFHs could be a product of local environmental effects such as non-uniform patchy reionization or stripping by the host (Martin et al. 2017).

in both CDM and WDM. WDM free-streaming effects weaken density perturbations on small scales, resulting in WDM haloes forming with a decreased central density, or equivalently, a smaller peak $V_{\rm max}$. The reduction in WDM central density relative to CDM is approximately the same for all haloes with a density ratio ranging from $\rho_{\rm WDM}/\rho_{\rm CDM}(r = 500\,{\rm pc}) = 0.60$–$0.75$ and a mean value of 0.70.

(ii) The stellar mass of a galaxy at $z = 0$ is correlated with its host halo's central density (or $V_{\rm max}(z_{\rm f})$) at the time of formation, where $z_{\rm f}$ is defined as the redshift where the $V_{\rm max}$ function initially reaches a value of $0.85\,V_{\rm max}(z = 0)$. The WDM haloes follow the same $M_\star(z = 0)$–$V_{\rm max}(z_{\rm f})$ trend as the CDM haloes owing to a similar degree of central density reduction from free-streaming effects amongst our WDM haloes.

(iii) Our suite of WDM dwarf galaxies can be divided into two groups based on stellar mass: WDM haloes with $V_{\rm max}(z_{\rm f}) > 25\,{\rm km\,s^{-1}}$ all have $M_\star \gtrsim 2 \times 10^6\,{\rm M}_\odot$. WDM haloes with $V_{\rm max}$ below this threshold form far fewer or no stars. These haloes are strongly affected by reionization feedback, as they have shallow central potentials that are barely capable of accreting and cooling warm ($T_{\rm IGM} \sim 2 \times 10^4$ K) gas in order to form stars.

(iv) The galaxy scaling relations follow the same trends in WDM as in CDM. Given a galaxy of a fixed mass, shape, and size, it is not possible to identify whether the halo is made up of warm or cold dark matter. All WDM galaxies feature a delay in the onset of star formation due to the later halo collapse times. As a result, all of the WDM galaxies studied here are devoid of stars formed before $z = 7$ and contain a significantly smaller fraction of stellar mass formed at early times relative to their CDM counterparts.

While our WDM simulation suite includes an ultrafaint galaxy with some ancient (reionization-era) star formation, there are no ultrafaint galaxies with an entirely old stellar population in this suite. Moreover, we predict a population of extremely young, gas-rich, actively star forming ultrafaint dwarfs that have formed over 80 per cent of their stars in the last 4 Gyr if dark matter is warm. Both WDM and CDM predict that some $M_{\rm halo} = 10^{10}\,{\rm M}_\odot$ haloes will not be able to form any stars.

(v) Free-streaming reduces the central densities of dwarf WDM haloes relative to their CDM counterparts. Feedback from bursty star formation further reduces the central density of WDM haloes; this effect is also present in CDM simulations. The CDM analogues host more massive galaxies and have more significant feedback events; the CDM galaxies therefore tend to have a greater impact on their haloes' central densities compared to their WDM counterparts when isolating the effects of stellar feedback from free-streaming. In one case, however, stellar feedback is more effective at reducing the central density in WDM than in CDM despite a smaller stellar mass and abbreviated SFH for the WDM galaxy. While the extra reduction is a modest $\sim$10 per cent, this demonstrates that larger modification of WDM haloes relative to CDM is possible in hydrodynamical simulations for WDM haloes with extended SFHs and low central densities.

(vi) Only half of our suite of WDM galaxies form stars before $z = 6$ and none of the haloes form stars before $z = 7$. These WDM galaxies contribute negligibly to the ionizing photon background, contrary to the expectations for galaxies in haloes at this mass scale in CDM. Previous studies have shown that WDM models with a similar free-streaming scale as the S229 model we study here are able to complete reionization by $z = 6$ through vigorous star formation in haloes with $M_{\rm halo} > 10^{10}\,{\rm M}_\odot$ (Schultz et al. 2014; Bose et al. 2016b; Villanueva-Domingo et al. 2018). The ability of these models to match high-z UV luminosity functions and the implications for galaxy formation in larger mass WDM haloes is left for future work.

We have demonstrated the viability of a resonantly-produced sterile neutrino WDM model to produce realistic dwarf galaxies and to simultaneously address small-scale issues found in the CDM paradigm. Our suite of WDM haloes features density profiles that are less centrally dense than their CDM counterparts, which is important for addressing the TBTF problem. A colder model and/or higher-mass haloes may see even larger reductions in the central density. A colder resonantly-produced sterile neutrino WDM model may also provide a better fit to constraints from reionization and SFHs of Local Group ultrafaint dwarfs. We will consider such models through FIRE simulations in a future paper.

ACKNOWLEDGEMENTS

MBK and AF acknowledge support from NSF grant AST-1517226. MBK was also partially supported by NASA grants NNX17AG29G and *HST*-AR-13888, *HST*-AR-13896, *HST*-AR-14282, *HST*-AR-14554, *HST*-GO-12914, and *HST*-GO-14191 from the Space Telescope Science Institute, which is operated by AURA, Inc., under NASA contract NAS5-26555. KNA is supported by NSF Theoretical Physics Grant No. PHY-1620638. DK was supported by NSF grant AST-1715101 and the Cottrell Scholar Award from the Research Corporation for Science Advancement. Support for SGK was provided by NASA through Einstein Postdoctoral Fellowship grant number PF5-160136 awarded by the Chandra X-ray Center, which is operated by the Smithsonian Astrophysical Observatory for NASA under contract NAS8-03060. CAFG was supported by NSF through grants AST-1412836, AST-1517491, AST-1715216, and CAREER award AST-1652522, by NASA through grant NNX15AB22G, and by a Cottrell Scholar Award from the Research Corporation for Science Advancement.

REFERENCES

Abazajian K. N., 2014, Phys. Rev. Lett., 112, 161303
Abazajian K. N., 2017, Phys. Rep., 711, 1
Anderhalden D., Schneider A., Macciò A. V., Diemand J., Bertone G., 2013, J. Cosmol. Astropart. Phys., 3, 014
Angulo R. E., Hahn O., Abel T., 2013, MNRAS, 434, 3337
Avila-Reese V., Colín P., Valenzuela O., D'Onghia E., Firmani C., 2001, ApJ, 559, 516
Barkana R., Haiman Z., Ostriker J. P., 2001, ApJ, 558, 482
Benítez-Llambay A. et al., 2017, MNRAS, 465, 3913
Benson A. J., Frenk C. S., Lacey C. G., Baugh C. M., Cole S., 2002, MNRAS, 333, 177
Bode P., Ostriker J. P., Turok N., 2001, ApJ, 556, 93
Bose S., Hellwing W. A., Frenk C. S., Jenkins A., Lovell M. R., Helly J. C., Li B., 2016a, MNRAS, 455, 318
Bose S., Frenk C. S., Hou J., Lacey C. G., Lovell M. R., 2016b, MNRAS, 463, 3848
Boyarsky A., Ruchayskiy O., Iakubovskyi D., Franse J., 2014, Phys. Rev. Lett., 113, 251301
Boyarsky A., Franse J., Iakubovskyi D., Ruchayskiy O., 2015, Phys. Rev. Lett., 115, 161301
Boylan-Kolchin M., Bullock J. S., Kaplinghat M., 2011, MNRAS, 415, L40
Boylan-Kolchin M., Bullock J. S., Kaplinghat M., 2012, MNRAS, 422, 1203
Bozek B., Marsh D. J. E., Silk J., Wyse R. F. G., 2015, MNRAS, 450, 209
Bozek B., Boylan-Kolchin M., Horiuchi S., Garrison-Kimmel S., Abazajian K., Bullock J. S., 2016, MNRAS, 459, 1489
Brooks A. M., Papastergis E., Christensen C. R., Governato F., Stilp A., Quinn T. R., Wadsley J., 2017, ApJ, 850, 97
Brown T. M. et al., 2014, ApJ, 796, 91

Bryan G. L., Norman M. L., 1998, ApJ, 495, 80
Bulbul E., Markevitch M., Foster A., Smith R. K., Loewenstein M., Randall S. W., 2014, ApJ, 789, 13
Bullock J. S., Boylan-Kolchin M., 2017, ARA&A, 55, 343
Bullock J. S., Kravtsov A. V., Weinberg D. H., 2000, ApJ, 539, 517
Chan T. K., Kereš D., Oñorbe J., Hopkins P. F., Muratov A. L., Faucher-Giguère C.-A., Quataert E., 2015, MNRAS, 454, 2981
Cole A. A. et al., 2007, ApJ, 659, L17
Cole A. A., Weisz D. R., Dolphin A. E., Skillman E. D., McConnachie A. W., Brooks A. M., Leaman R., 2014, ApJ, 795, 54
Colín P., Avila-Reese V., Valenzuela O., 2000, ApJ, 542, 622
Colín P., Avila-Reese V., González-Samaniego A., Velázquez H., 2015, ApJ, 803, 28
D'Onghia E., Springel V., Hernquist L., Keres D., 2010, ApJ, 709, 1138
Dalcanton J. J., Hogan C. J., 2001, ApJ, 561, 35
Di Cintio A., Brook C. B., Macciò A. V., Stinson G. S., Knebe A., Dutton A. A., Wadsley J., 2014a, MNRAS, 437, 415
Di Cintio A., Brook C. B., Dutton A. A., Macciò A. V., Stinson G. S., Knebe A., 2014b, MNRAS, 441, 2986
Diemand J., Kuhlen M., Madau P., 2007, ApJ, 667, 859
Efstathiou G., 1992, MNRAS, 256, 43P
Einasto J., 1965, Tr. Astrofiz. Inst. Alma-Ata, 5, 87
Famaey B., McGaugh S. S., 2012, Living Rev. Relativ., 15, 10
Faucher-Giguère C.-A., Lidz A., Zaldarriaga M., Hernquist L., 2009, ApJ, 703, 1416
Fitts A. et al., 2017, MNRAS, 471, 3547
Fitts A. et al., 2018, MNRAS, 479, 319
Flores R. A., Primack J. R., 1994, ApJ, 427, L1
Frenk C. S., White S. D. M., 2012, Ann. Phys., Lpz., 524, 507
Gao L., Springel V., White S. D. M., 2005, MNRAS, 363, L66
Garrison-Kimmel S. et al., 2017b, MNRAS, 471, 1709
Garrison-Kimmel S., Bullock J. S., Boylan-Kolchin M., Bardwell E., 2017a, MNRAS, 464, 3108
Gilmore G., Wilkinson M., Kleyna J., Koch A., Evans W., Wyse R. F. G., Grebel E. K., 2007, Nucl. Phys., 173, 15
González-Samaniego A., Avila-Reese V., Colín P., 2016, ApJ, 819, 101 (GS16)
Governato F. et al., 2012, MNRAS, 422, 1231
Governato F. et al., 2015, MNRAS, 448, 792
Hahn O., Abel T., 2011, MNRAS, 415, 2101
Herpich J., Stinson G. S., Macciò A. V., Brook C., Wadsley J., Couchman H. M. P., Quinn T., 2014, MNRAS, 437, 293
Hoeft M., Yepes G., Gottlöber S., Springel V., 2006, MNRAS, 371, 401
Hogan C. J., Dalcanton J. J., 2000, Phys. Rev., 62, 063511
Hopkins P. F. et al., 2018, MNRAS, 480, 800
Hopkins P. F., 2017, preprint (arXiv:1712.01294)
Hopkins P. F., Kereš D., Oñorbe J., Faucher-Giguère C.-A., Quataert E., Murray N., Bullock J. S., 2014, MNRAS, 445, 581
Horiuchi S., Bozek B., Abazajian K. N., Boylan-Kolchin M., Bullock J. S., Garrison-Kimmel S., Onorbe J., 2016, MNRAS, 456, 4346
Iakubovskyi D. A., 2016, Adv. Astron. Space Phys., 6, 3
Kirby E. N., Bullock J. S., Boylan-Kolchin M., Kaplinghat M., Cohen J. G., 2014, MNRAS, 439, 1015
Klypin A., Kravtsov A. V., Valenzuela O., Prada F., 1999, ApJ, 522, 82
Knollmann S. R., Knebe A., 2009, ApJS, 182, 608
Kravtsov A. V., Gnedin O. Y., Klypin A. A., 2004, ApJ, 609, 482
Kuhlen M., Vogelsberger M., Angulo R., 2012, Phys. Dark Universe, 1, 50
Larson D. et al., 2011, ApJS, 192, 16
Livermore R. C., Finkelstein S. L., Lotz J. M., 2017, ApJ, 835, 113
Lovell M. R. et al., 2012, MNRAS, 420, 2318
Lovell M. R. et al., 2017b, MNRAS, 468, 4285
Lovell M. R., Frenk C. S., Eke V. R., Jenkins A., Gao L., Theuns T., 2014, MNRAS, 439, 300
Lovell M. R., Gonzalez-Perez V., Bose S., Boyarsky A., Cole S., Frenk C. S., Ruchayskiy O., 2017a, MNRAS, 468, 2836
Lunnan R., Vogelsberger M., Frebel A., Hernquist L., Lidz A., Boylan-Kolchin M., 2012, ApJ, 746, 109
Ma X. et al., 2018, MNRAS, 477, 219
Macciò A. V., Paduroiu S., Anderhalden D., Schneider A., Moore B., 2012, MNRAS, 424, 1105
Martin N. F. et al., 2017, ApJ, 850, 16
Moore B., 1994, Nature, 370, 629
Moore B., Ghigna S., Governato F., Lake G., Quinn T., Stadel J., Tozzi P., 1999, ApJ, 524, L19
Moster B. P., Naab T., White S. D. M., 2013, MNRAS, 428, 3121
Munshi F. et al., 2013, ApJ, 766, 56
Munshi F., Brooks A. M., Applebaum E., Weisz D. R., Governato F., Quinn T. R., 2017, preprint (arXiv:1705.06286)
Noh Y., McQuinn M., 2014, MNRAS, 444, 503
Oh S.-H., Brook C., Governato F., Brinks E., Mayer L., de Blok W. J. G., Brooks A., Walter F., 2011, AJ, 142, 24
Okamoto T., Gao L., Theuns T., 2008, MNRAS, 390, 920
Oñorbe J., Boylan-Kolchin M., Bullock J. S., Hopkins P. F., Kereš D., Faucher-Giguère C.-A., Quataert E., Murray N., 2015, MNRAS, 454, 2092
Planck Collaboration XIII, 2016, A&A, 594, A13
Polisensky E., Ricotti M., 2011, Phys. Rev., 83, 043506
Power C., Navarro J. F., Jenkins A., Frenk C. S., White S. D. M., Springel V., Stadel J., Quinn T., 2003, MNRAS, 338, 14
Primack J. R., 2015, preprint (arXiv:1505.02821)
Read J. I., Agertz O., Collins M. L. M., 2016, MNRAS, 459, 2573
Ricotti M., 2009, MNRAS, 392, L45
Robles V. H. et al., 2017, MNRAS, 472, 2945
Sawala T. et al., 2016, MNRAS, 457, 1931
Sawala T., Frenk C. S., Crain R. A., Jenkins A., Schaye J., Theuns T., Zavala J., 2013, MNRAS, 431, 1366
Sawala T., Pihajoki P., Johansson P. H., Frenk C. S., Navarro J. F., Oman K. A., White S. D. M., 2017, MNRAS, 467, 4383
Schneider A., Smith R. E., Macciò A. V., Moore B., 2012, MNRAS, 424, 684
Schneider A., Smith R. E., Reed D., 2013, MNRAS, 433, 1573
Schultz C., Oñorbe J., Abazajian K. N., Bullock J. S., 2014, MNRAS, 442, 1597
Shao S., Gao L., Theuns T., Frenk C. S., 2013, MNRAS, 430, 2346
Shen S., Madau P., Conroy C., Governato F., Mayer L., 2014, ApJ, 792, 99
Shi X., Fuller G. M., 1999, Phys. Rev. Lett., 82, 2832
Skillman E. D. et al., 2014, ApJ, 786, 44
Smith R. E., Markovic K., 2011, Phys. Rev., 84, 063507
Somerville R. S., 2002, ApJ, 572, L23
Sommer-Larsen J., Dolgov A., 2001, ApJ, 551, 608
Tollet E. et al., 2016, MNRAS, 456, 3542
Tremaine S., Gunn J. E., 1979, Phys. Rev. Lett., 42, 407
van den Bosch F. C., Ogiya G., Hahn O., Burkert A., 2018, MNRAS, 474, 3043
Venumadhav T., Cyr-Racine F.-Y., Abazajian K. N., Hirata C. M., 2016, Phys. Rev., 94, 043515
Villaescusa-Navarro F., Dalal N., 2011, J. Cosmol. Astropart. Phys., 3, 024
Villanueva-Domingo P., Gnedin N. Y., Mena O., 2018, ApJ, 852, 139
Walker M. G., Peñarrubia J., 2011, ApJ, 742, 20
Wang J., White S. D. M., 2007, MNRAS, 380, 93
Wechsler R. H., Bullock J. S., Primack J. R., Kravtsov A. V., Dekel A., 2002, ApJ, 568, 52
Weisz D. R., Dolphin A. E., Skillman E. D., Holtzman J., Gilbert K. M., Dalcanton J. J., Williams B. F., 2014, ApJ, 789, 148
Wetzel A. R., Hopkins P. F., Kim J.-h., Faucher-Giguère C.-A., Kereš D., Quataert E., 2016, ApJ, 827, L23
Wheeler C. et al., 2017, MNRAS, 465, 2420
Wright A. C., Brooks A. M., Weisz D. R., Christensen C. R., 2019, MNRAS, 482, 1176
Zhao D. H., Mo H. J., Jing Y. P., Börner G., 2003, MNRAS, 339, 12
Zolotov A. et al., 2012, ApJ, 761, 71

This paper has been typeset from a TEX/LATEX file prepared by the author.